EUROPEAN FUSION DEVELOPMENT AGREEMENT

EFDA–JET–PR(05)38

V.G. Kiptily, F.E. Cecil, S.S. Medley and JET EFDA contributors

Gamma Ray Diagnostics of High Temperature Fusion Plasmas

Gamma Ray Diagnostics of High Temperature Fusion Plasmas

V.G. Kiptily[1], F.E. Cecil[2], S.S. Medley[3] and JET EFDA contributors*

[1]EURATOM/UKAEA Fusion Association, Culham Science Centre, Abingdon, OX14 3DB, UK
[2]Colorado School of Mines, Golden 80401, USA
[3]Princeton Plasma Physics Laboratory, Princeton 08544, USA
** See annex of J. Pamela et al, "Overview of JET Results ", (Proc. 20th IAEA Fusion Energy Conference, Vilamoura, Portugal (2004)).*

Preprint of Paper to be submitted for publication in
Plasma Physics and Controlled Fusion

ABSTRACT

We present a review of the use of gamma ray spectrometry as a diagnostic of nuclear reaction rates and nuclear reaction product densities in high temperature fusion plasmas. In this review we will discuss the historic genesis of the concept, a brief overview of the relevant nuclear physics, the experimental techniques utilised in the measurements and some of the analytical techniques required to extract the diagnostic information from the basic measurements. Of particular interest is the ability to measure the population of confined fast alpha particles in future burning plasma experiments.

INTRODUCTION

For fusion plasma experiments, which are dedicated to the ultimate utilization of controlled nuclear fusion as an energy source, the rates at which the energy producing reactions occur are, perhaps, the best indicators of this energy production. The measurement of these rates thus represents an essential diagnostic of these experiments. The quantitative spectrometry of high energy (MeV) gamma rays from nuclear reactions within the plasma offers an opportunity of determining these rates which is complementary to neutron flux measurements in the case of neutron producing reactions such as in *DD* or *DT* plasmas or which is unique in the case of aneutronic reactions such as occur in *HD*, *HT*, D^3He or advanced fuel scenarios such as *H-Li* or *H-B* plasmas. Indeed for such plasmas gamma ray spectrometry offers, perhaps, the only direct measure of the nuclear reaction rates and, in this sense, is analogous to the use of solar neutrinos to measure the rate of nuclear reactions at the centre of the sun. Of comparable importance to nuclear reaction rates in the present generation of *DT* experiments and future burning plasma experiments is the behaviour of the fusion reaction products. Of particular interest is the behaviour of the alpha particles from the *DT* or D^3He reactions as their confinement is crucial to the heating of these plasmas. As with the reactions among the primary constituents of the plasma, gamma ray spectrometry among reactions between the fusion product alpha particles and other plasma constituents, including impurities in the plasma, provides a basis for the measurement of the energy spectrum of these confined alpha particles. In this review we will discuss the basic phenomenology of the gamma ray production, some of the techniques of gamma ray spectrometry and applications of this spectrometry as a diagnostic of fusion plasmas.

In the next section we discuss the historical genesis and development of the concept of fusion gamma ray diagnostics including examples of measurements of fusion gamma rays at various tokamak facilities and the accelerator-based measurements of the relevant reaction cross sections. Following this we present an overview of the basic nuclear physics governing the reactions, the phenomenology required to translate this nuclear physics into a predicted gamma ray production rate and techniques that have been developed to measure the energy and fluence of the gamma rays. In the following section we discuss the application of this phenomenology and these techniques to the diagnostics of specific fusion plasma parameters in realistic tokamak environments and briefly address the recent application of gamma ray spectrometry to the diagnostics of inertial confinement

fusion plasmas. In the concluding section, we speculate on application of fusion gamma ray spectrometry to future problems of fusion plasma diagnostics.

1. HISTORICAL DEVELOPMENT

The use of nuclear gamma ray spectrometry as a diagnostic tool has been evolving for a number of decades. In their review of the diagnostics of intense pulsed ion beams, Young et al. [1] note the potential for the radiative capture reaction $^{12}C(p,\gamma)^{13}N$ as the basis for determining the energy and fluence of a proton beam. Medley and Hendel [2] later proposed the specific gamma ray producing reactions $d(t,\gamma)^5He$ and $d(^3He,\gamma)^5Li$ as potential diagnostics of tokamak fusion plasmas. Cecil and Newman [3] then suggested a measurement of the energy and width of the gamma ray lines from the fusion reactions among the isotopes of hydrogen (p, d, and t) that are independent of the ion densities as a method for determining the temperatures of thermonuclear hydrogen plasmas.

The first observations of nuclear reaction gamma rays from fusion plasmas were reported by Newman and Cecil [4] who measured the 5.5 MeV gamma rays from the $d(p,\gamma)^3He$ reaction during hydrogen neutral beam heated deuterium plasmas on Doublet-III. At this juncture it was realized by several groups that there were no reliable measurements of the cross sections for a number of these reactions at the appropriate low energies (~100keV). Measurements of these reactions were subsequently reported by Cecil and Wilkinson [5], Morgan et al. [6] and Kammerad et al. [7] for the reaction $d(t,\gamma)^5He$, Cecil et al. [8] for the reaction $d(^3He,\gamma)^5Li$ and Wilkinson and Cecil [9] and Barnes et al. [10] for the reaction $d(d,\gamma)^4He$.

The measurement of the $d(^3He,\gamma)^5Li$ reaction cross section allowed a quantitative study of the total reaction rate during d-^{3}He fusion plasmas. Sadler et al [11] and later Boyd et al. [12] observed these gamma rays during ICRH ^{3}He minority heating of deuterium plasmas on JET. Cecil and Medley observed these gamma rays during deuterium neutral beam heated ^{3}He plasmas on TFTR [13] as did Nishitani et al on JT-60. [14]

Measurements of the cross sections for (p,γ) reactions by Cecil et al. [15] on the stable isotopes of Li, Be and B made possible the calculations of the reaction rates for the corresponding advanced fuel fusion plasmas [16].

The above examples all involve the primary constituents of the plasma. In addition, considerable effort has been devoted to utilizing the spectrometry of the gamma rays produced by reactions between fusion products and plasma impurities and reactions between the primary constituents and plasma impurities. Cecil, Zweben and Medley [17] calculated the yields of gamma rays from the resonant interactions between fusion product alpha particles and the ^{6}Li and ^{7}Li impurities as a diagnostic of fast confined alpha particles. Kiptily et al. [18] similarly proposed the reaction $^9Be(\alpha,n\gamma)^{12}C$ as diagnostic of fast confined alpha particles. Jarvis et al. [19] and later Kiptily [20] looked at the gamma rays from the interactions between ICRH heated ^{3}He ions and the ^{9}Be and ^{12}C impurities on JET to generate 2-D tomographic gamma-ray emission profiles as a diagnostic of the spatial dependence of the ICRH heating. Most recently, Kiptily et al. have

observed the gamma rays from the $^{9}Be(\alpha,n\gamma)^{12}C$ reaction during ICRH heating of ^{4}He neutral beam-ions in plasmas on JET [21] and measured 2-D gamma-ray emissivity [22]. This reaction has most recently been used by Kiptily et al. to observe fusion product alpha particles during JET's recent trace tritium experiments [23].

NUCLEAR PHYSICS OF FUSION GAMMA RAYS

In this section we look at some of the nuclear reactions which have provided the basis for fusion gamma ray spectrometry as a plasma diagnostic. We will specifically look at the energies of the gamma rays, and the yields of the gamma rays in thermonuclear, neutral beam and ICRH plasmas and for fusion product alpha particles in the presence of hydrogenic plasmas in which impurities such as carbon or beryllium may be present. These gamma rays are one of the final state products of two-body initial state nuclear reactions initiated by the atomic or ionic constituents of the plasma. These reactions may be direct (one-step) reactions such as:

$$d + t \rightarrow \gamma + {}^{5}He \qquad (1)$$

or compound (two-step) reactions such as:

$$\alpha + {}^{9}Be \rightarrow {}^{12}C(4.44\ MeV) + n \text{ followed by } {}^{12}C(4.44\ MeV) \rightarrow \gamma + {}^{12}C \qquad (2)$$

where the excitation energy of the intermediate excited nuclear state of the compound ^{12}C nucleus is indicated parenthetically.

The energies of the gamma rays are determined by the simultaneous requirement of energy and momentum conservation during the reactions. (The phenomenology described in this section is developed in Reference 3). For the generic reaction:

$$M_1 + M_2 \rightarrow M_3 + \gamma \qquad (3)$$

$$E_\gamma = E_0 + Q\,(1 - Q/(2\,M_3))\,(1 + 2\,(v_{CM}/c)\,\mathrm{Cos}\,(\theta)) \qquad (4)$$

where: $Q = M_1 + M_2 - M_3$ with the M's being the rest energies of the masses

$E_0 = E_1 + E_2$ being the sum of the centre of mass kinetic energies of the reactants

v_{CM} = the speed of the centre of mass of the reactants relative to the observer

θ = the angle of the gamma ray in the coordinate system of the observer relative to the direction of the centre of mass motion of the initial reactants

In Eq. (4), we assume non-relativistic expressions for the kinetic energies and momenta of the reactants and more generally $E_i << Q << M_i$. This approximation is well satisfied for the plasma conditions currently under consideration; e.g for the $d + t \rightarrow \gamma + {}^{5}He$ reaction noted above, assuming a thermal plasma with a temperature of 10^8 K (kT = 8.3keV), the bulk of the plasma constituents will have a kinetic energy in the range of 10 keV, the Q value for the reaction is about 16 MeV while the rest mass energies of the reactants are several GeV.

Equation (4) gives the energy of the gamma ray in terms of the energies of the initial reactants. In a thermal plasma, the energies of the reactants are characterized by a Maxwell-Boltzmann distribution which has its maximum at an energy kT/2. However, the reactant energies that dominate the reaction are not necessarily those at the peak of the thermal distribution. At the energies encountered in current plasma experiments, the reactants have energies well below the Coulomb barrier separating them. Consequently the reaction cross sections are rapidly falling as the energies approach zero. Indeed the energy dependence of the cross sections is roughly that of the quantum mechanical Coulomb barrier penetration probability:

$$\sigma(E) = S(E)/E \; e^{-(b/\sqrt{E})} \text{ where:} \qquad (5)$$

S(E) is the†"astrophysical S-factor" which, in the absence of narrow resonances, is a slowly varying function of energy and $b = 31.28 \, Z_1 \, Z_2 \, A^{1/2}$ keV$^{1/2}$ with Z the atomic number and A the reduced atomic weight in units of amu.

The number of gamma ray producing reactions per unit volume is then:

$R = n_1 \, n_2 \, (1 + \partial_{12})^{-1} \langle \sigma \, v \rangle$ where n_1 and n_2 are the densities of the reactants, ∂_{12} is equal to unity for identical species or is equal to zero for different species and the reactivity $\langle \sigma v \rangle$ is the integral of the velocity weighted product of the cross section and the population distribution, e.g. a thermal distribution

$$\langle \sigma v \rangle = \int v(E) \, \sigma(E) \, n(E) \, dE \qquad (6)$$

Because, as noted above, the cross section drops at low energies, the energy at which the integrand in (6) is a maximum is above the peak in the distribution. For a thermal distribution, this energy maximum is referred to as the Gamow peak which physically is the maximum overlap of the distribution dropping at high energies and the cross section dropping at low energies and which assumes the value:

$$E_G = (\pi \, \alpha \, Z_1 \, Z_2 \, k \, T)^{2/3} \, (M_1 \, M_2 / (M_1 + M_2))^{1/3} \qquad (7)$$

with α the fine structure constant. The width (fwhm) of this peak similarly may be shown to be

$$\Delta E_G = (16 \, E_G \, kT/3 + 5.4 \, Q^2 \, kT/M_3)^{1/2} \qquad (8)$$

Numerically for a *DT* plasma with a temperature of 10^8 K (kT = 8.3keV), Eg = 32 keV (well above the peak in the population distribution of 4.2keV), ΔE_G = 41keV and $\langle \sigma v \rangle = 4.3 \, 10^{-21}$ cm^3 s^{-1}. Hence for a deuteron and triton density of 10^{13} cm^{-3}, the gamma ray yield will be $4.3 \, 10^5$ cm^{-3} s^{-1}. The energies of the observed gamma rays will thus be in an approximately symmetric distribution with the centroid of the distribution at:

$$E_\gamma = Q \, (1 - Q/(2 \, M_3)) + E_G \qquad (9)$$

and the width of the distribution being the combined width due to the Doppler broadening (the average over the Cos(θ) factor in Eq. (4)), the width of the Gamow peak (Eq. (9)) and the intrinsic

width of the ground state ì of the final product nucleus: in the case of the $d + t \rightarrow \gamma + {}^{5}He$, the width Γ of the ^{5}He ground state is 600 keV. In order to calculate reaction rates for non-thermal plasmas, such as neutral beam heated or ion cyclotron resonance heated plasmas, the population distribution n(E) in Eq. 6 would have to be appropriately modified

The Q values, S factors (extrapolated to zero energy) and final product ground state widths of possible fusion gamma ray diagnostic reactions are given in Table 1. The phenomenology associated with the fusion gamma rays from compound nuclear reactions is basically the same as that for the direct reactions with the important exception that there can be narrow resonances in the capture cross section. These are discussed in greater detail in Reference 24.

2. DETECTION OF FUSION GAMMA RAYS

In this section, we will review some of the instrumentation and analytical techniques used in the measurement of fusion gamma rays.

The fusion gamma-ray spectra recorded at Doublet-III [4] employed a detector which consisted of a 5cm diameter × 5cm long NaI(Tl) crystal viewed by a Photo-Multiplier Tube (PMT). The detector was placed in a lead collimator 4 m from the machine centre viewing the plasma tangentially. An 8mm lead cover in front of the collimator eliminated plasma hard X-rays and low energy gammas. The PMT pulses were recorded in a multi-channel pulse-height analyser. During neutral proton beam injection, 5.5MeV gammas from the reaction $D(p,\gamma)^{3}He$ were observed.

On TFTR, NaI(Tl) and NE226 detectors were used for gamma-ray measurements [13]. The detectors were enclosed in compact blockhouse on the test cell floor having overall dimensions approximately 2m wide by 2m long by 1m high and consisting of nested strata of concrete, polyethylene, lithium carbonate, and lead. The detectors viewed the TFTR vacuum vessel through a 1.5m long by 20cm diameter cylindrical collimator in the blockhouse. The 10cm diameter by 10-cm high NaI(Tl) crystal scintillator was used for background gamma-ray measurements. The fusion gammas during deuterium Neutral Beam Injection (NBI) heating of ^{3}He plasmas were observed by means of a 12.7cm long by 12.7cm diameter cylindrical cell of liquid fluorocarbon scintillator NE226. This is a neutron insensitive scintillator with rapid decay constant ($\approx$ 2ns), and the peak energy resolution and detection efficiency for gamma rays up to 19MeV have been reported [25]. This gamma-ray spectrometer on TFTR was interfaced to 16 single-channel analysers and demonstrated a count rate capability in excess of 10MHz [26].

In the JET tokamak, gamma-ray energy spectra are measured with two different devices, one with a horizontal and one with a vertical line of sight through the plasma centre [20]. The first spectrometer is a calibrated bismuth germanate (BGO) scintillation detector with diameter 75mm and a height 75mm that is located in a well-shielded bunker and views the plasma tangentially. In order to reduce the neutron flux and the gamma-ray background, the front collimator is filled with polythene. Behind the scintillation detector there is an additional dump of polythene and lead. The gamma rays are continuously recorded in all JET discharges over the energy range 1-28MeV, with

an energy resolution of about 4% at 10MeV. The second device for the gamma-ray energy spectrum measurements is a NaI(Tl) scintillation detector with a diameter of 125mm and a height of 150 mm, viewing the plasma vertically through the centre.

The spatial distribution of the gamma-ray emission sources in the JET plasma is measured using the neutron profile monitor [27], which is routinely used for the neutron and gamma-ray measurements. The monitor consists of two cameras, vertical and horizontal, with 9 and 10 lines of sight, respectively. The radiation detectors are NE213 liquid scintillators. Although the JET profile monitor was developed for neutron measurements and the shielding and detectors are not entirely adequate for gamma-ray measurements, in some discharges with ICRF-only heating the gamma-ray measurements are possible by exploiting the different pulse shape characteristics exhibited by NE213 for neutrons and gamma-rays [19, 20]. The standard pulse-shape-discrimination electronic modules were set up to restrict the detection of the gamma-ray emission to the energy range 1.8-6 MeV. It was shown that the discrimination between the gamma rays produced by ICRF-accelerated fast ions and the neutrons is acceptable for further analysis if their count rates are compatible.

Now at JET, to measure the γ-ray emission profile in the energy range E_γ>26MeV we use the fast-electron-bremsstrahlung diagnostic system, which is incorporated into the neutron profile monitor. As with the neutron profile monitor, the gamma cameras have horizontal and vertical shielded fan-like arrays of lines of sight (Figure 1). The detector array is comprised of the 19 *CsI(Tl)* photo-diodes (10mm × 10mm × 15mm). For measurements the photo-diodes are remotely placed in the front of neutron detectors within each collimation channel. The *CsI(Tl)* detectors are well calibrated with radioactive sources ^{22}Na (511, 1275keV), which are embedded in the neutron detector-array module. The data acquisition system accommodates the γ-ray count-rate measurement in four energy windows. This allows allocating specific γ-ray peaks in the windows to be counted separately [23].

It will be necessary to develop optimal gamma-detectors and shielding to reduce radiation background effect in future fusion reactors. To implement the optimal background conditions for the gamma-diagnostics there are some interesting detector ideas. A large scintillation spectrometer with an active annular veto detector has been installed in JET [28]. The system consists of a central 4" diameter by 5" high NaI(Tl) cylindrical scintillator surrounded by cylindrical NaI(Tl) annular scintillator of outside diameter 12", inside diameter 4" and height 8". This spectrometer was successfully used for fusion gamma-ray measurements during NBI and ICRH plasma heating.

An active background-suppressed multi-crystal spectrometer MULTICS was proposed in [29], which consists of a central HPGe-detector surrounded with 12 BaF_2-detectors. Monte-Carlo calculations have shown that the optimal detector efficiency will be in the case of the full energy summation mode.

Another multi-crystal spectrometer was developed as a full-energy-absorption spectrometer GAMMACELL [30]. It consists of nine, optically independent, scintillation BaF_2 detectors assembled in a single housing. The detector array functions as a full energy absorption spectrometer. The spectrometer is placed inside a radiation shielded blockhouse in such a way that gamma rays penetrate

through the collimator only onto the central section of the detector array. All these detectors are connected in a circuit ensuring summation of the full absorption energy of every gamma ray falling onto the central crystal. One more BaF_2 detector is installed in front of this crystal. This detector serves as an absorber of low-energy gamma rays and, simultaneously, as a rejecter of annihilation and scattered radiation that hit the central crystal. This substantially suppresses the background event-rate from the main detector. The dimension of the singe-crystal section is $W42 \times H42 \times L142$ mm. Maximum housing dimensions of the spectrometer are $D195 \times L360$ (Figure 2). The passive-active shielding detector is housed in the detached box that is separated from the main spectrometer by a lead backstop with a hole. In this detector the size of the BaF_2 crystal is $W60 \times H60 \times L40$ mm. The GAMMACELL has been optimized for measuring high-energy gamma rays (in the MeV range up to 30 MeV) for ITER-like reactors in the presence of high levels of low-energy background radiation and neutron fluxes.

A dedicated neutron absorber for fusion gamma-diagnostics was designed and fabricated [31]. When used to plug the pre-collimator, this absorber provides a high attenuation of neutron flux without significant losses of gamma-ray counts. The absorber is a hermetically sealed cylinder of 300mm length and 30mm diameter containing ^6LiH. Measurements of neutron attenuation and background were performed by means of neutron generator beams [31]. Attenuation factors of approximately 900 and 30 were found for 2.8MeV and 14.8MeV neutrons, respectively. Gamma-ray measurements at the JT-60U tokamak, during experiments with deuterium NB heated plasmas [32], showed that use of these plugs reduced the neutron-induced background by a factor of 10.

3. DIAGNOSTIC CAPABILITIES OF FUSION GAMMA RAY SPECTROMETRY

In this section, we will discuss the techniques whereby the spectrometry of the fusion gamma rays is used to infer fundamental properties of the corresponding plasmas.

3.1. TYPICAL GAMMA-RAY SPECTRA IN THE HOT TOKAMAK PLASMAS

There are three sources of fast particles that can give rise to a gamma-ray emission from JET plasmas. Firstly, fusion reactions between the plasma fuel ions produce fusion products such as fast tritons, protons, ^3He and ^4He ions with energies in the MeV range.

Secondly, ICRF heating of H and ^3He-minority ions accelerates these ions to energies in the MeV range [20, 21]. There are also ICRF schemes to accelerate D, T and ^4He ions [21, 22]. Thirdly, NBI heating introduces D, T, H, ^{4}He and/or ^{3}He ions.

Most simple gamma-ray spectra are usually observed in deuterium plasmas heated by deuterium NBI only. Due to the low energy with which the neutral beam ions are injected, the direct contribution from the NBI ions to the gamma-ray emission is small. However, beam-plasma and beam-beam nuclear reactions can amplify the yield of the charged fusion products and thereby contribute to the gamma-ray emission from the plasma. The fusion product neutrons interact with the structural

materials of JET, generating a continuous gamma-ray background. Fast ions born in fusion reactions produce line spectra due to their nuclear reactions with low-Z plasma impurities.

The gamma-ray energy spectra observed in ICRF-only discharges differ significantly from those observed in discharges with NBI-heating only. A typical spectrum for hydrogen minority ICRF-heating is shown in Figure 3. During this discharge, the hydrogen minority ions are accelerated up energies in the MeV range, and the first and second levels of the impurity ^{12}C nucleus are excited due to the inelastic scattering of the ICRF-driven protons. Combined NBI+ICRF plasma heating leads to more complicated gamma-ray spectra that require sophisticated analysis.
In order to identify the fast particles that exist in the plasma and give rise to the observed gamma-ray emission, and in order to assess the effective tail temperatures of these fast ions, a dedicated code for the gamma-ray spectrum modelling, the GAMMOD code, has been developed [20].

3.2. IMPORTANT NUCLEAR REACTIONS GIVING RISE TO GAMMA-RAY EMISSION

A list of all essential nuclear reactions, which have been identified in the gamma-ray spectra recorded at JET, is given in the Table 2. This is an extension of the fundamental direct capture reactions given in Table 1.These reactions are classified by the types of the fast ions interacting with different target ions in the plasma. The nuclear reaction energies, the *Q*-values, which characterise the mass balance of the reactions, are also presented there and can be used for an assessment of the excitation energy of the residual nuclei. The table also contains assessments of the minimum energy of the fast particles required to produce gamma-ray yields at levels that can be measured in JET.

Each gamma-ray spectrum depends on the type of reaction, the energy of the interacting particles and on the structure of the energy levels of the final nucleus. There are two types of reactions, which are most important for the diagnostics, i.e. threshold and resonant capture reactions. The inelastic scattering of protons on carbon, $^{12}C(p,p'\gamma)^{12}C$, is a typical threshold reaction which takes place in JET plasma with ICRF-heating tuned to hydrogen. Excitation of the first level of the nucleus ^{12}C, 4.44 MeV, is energetically allowed for protons with energies of 4.8MeV. However, due to the Coulomb interaction, the cross-section of the reaction only becomes noticeable for protons with energies above 5MeV. In order to excite the second level of the nucleus ^{12}C at 7.65MeV, the hydrogen ions have to be accelerated up to roughly 8 MeV. The reaction produces 3.21MeV gamma-rays by virtue of the sequential decay through the 4.44 MeV level and is indicated in the gamma-ray spectrum shown in Figure 3.

Another remarkable type of nuclear reaction, although exothermic, exhibits a threshold feature because its *Q*-value lies below the energy of the first excited state, for example $^{12}C(d,p\gamma)^{13}C$. Observation of gamma-rays de-exciting these states is evidence for the threshold crossing. In the case of the reaction $^{12}C(d,p\gamma)^{13}C$, the deuterons accelerated in JET with second harmonic ICRF-heating react with ^{12}C to yield ^{13}C in excited states with the energies 3.09, 3.68 and 3.85MeV. Observation of the gamma-rays de-exciting these levels requires necessarily deuterons with energies exceeding the threshold energies of 0.43, 1.12 and 1.32MeV, respectively. However, those deuterons

with energies close to the resonance energies of 0.9, 1.9 and 2.5 MeV, respectively, provide the main contribution to the gamma-line intensity.

There is an even more complex population of levels of the nucleus ^{14}N in the reaction $^{12}C(^{3}He,p\gamma)^{14}N$, which has also been observed in JET. The Q-value of this reaction is 4.78MeV and thus above the first two excited states at 2.31 and 3.95 MeV, but below those at 4.91 and 5.10 MeV. Only ^{3}He-ions accelerated to an energy of 1.3 MeV or greater can populate these states because of the high Coulomb barrier. However, a considerable population of even higher excited states of ^{14}N, including energy levels 6.20, 6.44 and 7.02MeV, occurs if the energy of the ^{3}He-ions exceeds 2MeV.

In the case of the resonant capture reactions, such as $^{9}Be(p,\gamma)^{10}B$, the intensities of the gamma-lines are proportional to the density of the fast ions at the resonant energies, which facilitates the fast particle analysis. In this particular reaction, the resonances at the proton energies 0.32, 1.0, 1.08 and 1.3MeV are strong, and corresponding gamma-rays have been observed. Another branch of this reaction is $^{9}Be(p,\alpha\gamma)^{6}Li$, which has a strong resonance at the proton energy of 2.57MeV producing 3.6MeV gammas.

Of the gamma-diagnostic nuclear reactions with protons which can take place in plasmas, the capture reaction $D(p,\gamma)^{3}He$ is very useful for the analysis of proton tail distributions below 400keV. The first observation of 5.5MeV gammas born in this reaction was made in the experiment performed with a 70keV hydrogen beam on Doublet-III [2] and later at JET [27, 19]. A typical spectrum measured during recent H-minority heating experiments in JET deuterium plasma, with a peak at the gamma energy of 5.5MeV due to gamma-ray emission from the $D(p,\gamma)^{3}He$ reaction, is shown in Figure 4. The effective temperature of the hydrogen tail in this discharge was assessed from the broadening of the gamma line at 5.5MeV to be about 0.20MeV using the GAMMOD code. Finally, Table 2 shows the reaction $^{9}Be(\alpha,n\gamma)^{12}C$, the significance of which was investigated in detail [18] for the fusion-born α–particle measurements. This is another type of resonant reaction, which also has thresholds. The presence of the 4.44MeV peak in the gamma-ray spectra is evidence for the existence of alphas with energies that exceed 2MeV. This reaction was successfully used at JET for the fast ^{4}He-ions [22] and fusion alpha-particle studies [23]. Comparable diagnostic reaction for ITER can be found in [34, 35].

3.3. GAMMA-RAY DIAGNOSIS OF FAST H *AND* D *DURING ICRF HEATING*

A typical example of the use of the reaction $^{12}C(p,p'\gamma)^{12}C$ in H-minority heating in JET tritium plasma is shown Figure 5 from [36]. This example is taken from a tritium discharge with $n_H/(n_H+n_D+n_T) \approx 5\%$ carried out in the JET 90%-tritium plasma with $P_{ICRF} \approx 8$MW tuned to a fundamental H resonance at $R_{res} \approx 3.12$m. The gamma-ray emission due to the reaction $^{12}C(p,p'\gamma)^{12}C$ is clearly visible in the gamma-ray energy spectrum, indicating the presence of ICRF-accelerated protons with energy exceeding 5MeV. This confirmed presence of high energy protons further permitted the threshold reaction $T(p,n)^{3}He$ to be identified as the source of 40% excess neutron emission in this discharge [36]. Since there is no indication of gamma-rays from the reaction $^{12}C(d,p\gamma)^{13}C$ in the measured gamma-ray energy spectrum, the surprisingly high neutron yield in

this discharge is unlikely to be due to the fast deuterons accelerated at their second harmonic resonance coinciding with the fundamental hydrogen resonance.

An example of a gamma ray spectrum showing a clear signature from fast deuterons during hydrogen minority heating is shown in Figure 4. As can be seen, there is not only a gamma-peak due to the capture reaction $D(p,\gamma)^3He$ but also due to the reaction $^{12}C(d,p\gamma)^{13}C$ in the spectrum. According to GAMMOD, the effective tail temperature of the hydrogen minority ions and deuterons is 0.20±0.05MeV and 0.1 MeV, respectively, and the fast deuterium population is three times lower than the hydrogen fast component

4. GAMMA-RAY OBSERVATION DURING ^3HE-MINORITY HEATING

The capabilities of the gamma-ray diagnostics are further demonstrated by the gamma ray spectrum produced by fast ^3He-ions [12,19,20,33]. As an example, the gamma-ray spectrum recorded during ^3He-minority heating plasma in JET [20] with high ^3He concentration $n_{He}/n_e \approx 20$ % is shown in Fig.6. In these conditions, not only was the above mentioned strong gamma emission from the reaction $^{12}C(d,p\gamma)^{13}C$ discussed above observed but also the 17MeV and 13MeV gamma-rays from the direct reactions $D(^3He,\gamma)^5Li$ to the ^{5}Li ground and very broad first excited states and 4.44MeV gamma-rays from the reaction $^{12}C(p,p'\gamma)^{12}C$ were detected. According to the GAMMOD modelling, the effective tail temperature of fast ^3He ions was below 100keV whereas the fast deuteron temperature is around 300keV. The low tail temperature of the ^3He ions is due to the high ^3He-concentration. In these conditions, the ICRF-power absorption by ^3He is small. However, some ICRF power has been clearly damped on the deuteron beam, as this is the only candidate for explaining the observed gamma emission from $^{12}C(d,p\gamma)^{13}C$. The relatively high gamma yield from the reaction $D(^3He,\gamma)^5Li$, which is the weak branch of the reaction $D(^3He,p)^4He$, can be explained by a high energy *D*-tail and high thermal density of ^3He ions. Finally, the peak of the gamma-ray intensity at energy 4.44MeV can only be explained by the presence of high energy protons (E_p>5MeV) giving rise to the gamma emission due to the threshold reaction $^{12}C(p,p'\gamma)^{12}C$. The most likely source of such energetic protons in these discharges is the fusion reaction $D(^3He,p)^4He$. Detailed information on the study of D^{3}He-fusion reaction has been published [12, 37]. An example of time evolution of the 17MeV γ-ray emission, which is used in JET as an indicator of the ICRF power deposition efficiency, is presented in Fig.7.

5. GAMMA-RAY OBSERVATION OF FAST ^4HE IONS IN ^4HE PLASMA

In a dedicated JET experiment [21,22] with the third harmonic heating of ^4He beam in ^4He plasma [38], the gamma radiation due to the reaction $^9Be(\alpha,n\gamma)^{12}C$ has been observed for the first time, showing the ICRF-acceleration of ^4He beam ions up to the energies in excess of 2MeV. When the ^4He-beam energy was increased from 70keV to 110keV in these experiments, thus increasing the single pass ^4He damping of the ICRF waves, the effective tail temperature increased typically from 0.5MeV to 1.3MeV. A strong gamma-ray emission from the reaction $^{12}C(d,p\gamma)^{13}C$ observed in the

experiments indicated that some ICRF power was also absorbed by the deuterium minority at the third harmonic *D* resonance which coincides with the third harmonic ^4He resonance. Figure 8 from [22] shows the γ-ray spectra recorded during 1s in two similar discharges with a high-resolution *NaI(Tl)* spectrometer. It is seen that when the 110keV neutral-beam heating injector was replaced by the 70-keV one with the same power, the intensity of the 4.44MeV γ-emission fell substantially whereas the deuterium γ-peak did not change. This effect can be explained by decreasing single pass ^4He damping of the ICRF waves due to the smaller value of the finite Larmor radius that determines the third harmonic absorption.

The relaxation of the distribution functions of fast ^4He and *D*-ions have been simultaneously studied during slowing down in ^4He-plasma [39]. For the measurements the 4.44MeV gammas from the $^9Be(\alpha,n\gamma)^{12}C$ reaction and 3.09MeV γ-rays from the $^{12}C(d,p\gamma)^{13}C$ reaction have been used. The γ-ray decay-time for both ions was measured during notches in the ICRH power when the accelerated ion source was strongly reduced. The γ-ray spectra with 100-ms integration time were recorded by means of a NaI-detector, which observes the plasma core through the vertical collimator. Figure 9 presents the measured γ-ray decay-times vs. classical slowing down time τ_{se}. The data derived from discharges with monotonic q-profiles. It is seen that the correlation $\tau_\gamma \sim 0.5\tau_{se}$ is observed, which could be explained by tail-like distribution function and T_e decreasing during the notch. An effect of the A/Z^2-factor for the classical slowing-down time is confirmed in these experiments.

6. FUSION ALPHA-PARTICLE MEASUREMENTS

The first γ-ray measurements of fusion-born α particles were carried out in JET 'trace tritium' discharges, i.e. in majority deuterium plasma after seeding with a small population of tritium Neutral Beam Injection (NBI) fast ions [23]. The γ-ray emission from the nuclear reaction $^9Be(\alpha,n\gamma)^{12}C$ is used to measure changes in the density of the fast α particles with energy $E_\alpha > 1.7$MeV in the post-NBI period. This important diagnostic nuclear reaction had already been applied to detect the presence of the fast α-particles in JET experiments, where ion-cyclotron-resonance heating of ^{4}He-beam ions was used to accelerate ^{4}He to the MeV range [20-22].

Clear variations in the intensity of the 4.44MeV γ-ray emission were observed in the post-beam-blip period of many discharges. Figure 10 shows decays of the 4.44MeV γ-ray intensity, recorded by the BGO-spectrometer in discharges with different NBI heating power. The measured rate of 14MeV neutrons, which are born during the T-beam injection, is shown as well. The main plasma heating (deuterium NBI) was kept constant for several seconds after the T NBI-blip, ensuring steady plasma conditions. The γ-ray decays are thus measured against unchanging plasma conditions. In these experiments the duration of T-beam blips was $t_{blip} \leq 300$ms.

In these experiments the time evolution of the MeV α-particle density was obtained, and a correlation between the decay-time of the γ-ray emission and the characteristic α particle slowing-down time in different plasma scenarios was established. The majority of the results are consistent with classical slowing-down of the MeV α particles and the parent tritons. However, in discharges

with low plasma current and in discharges with hollow current profiles the γ-ray emission was found to decay on a much shorter time-scale. This was attributed to wide orbit effects (enhanced losses and transport), which determine the α-particle behaviour, and this interpretation is consistent with preliminary theoretical predictions, which indicate that only larger machines with higher currents, can cope with the current hole effect on fusion-born α-particles.

7. GAMMA RAY TOMOGRAPHY

In addition to the measurements of the effective tail temperatures and the relative densities of different fast ion species that give rise to the gamma-emission, gamma-ray diagnostics can also provide information on the radial distribution of the fast ions. That can be done using a multi-collimator detector array like the 2-D system at JET, which has been described above. In this Section, we will illustrate this capability of gamma-ray tomography using the JET results.

The first 2-D profiles of the gamma radiation were derived by tomographic reconstruction in ^{3}He-minority ICRF heating experiments carried out by Jarvis [19]. It was found that the RF accelerated ions follow trapped orbits with turning points at the resonance layer, in conformity with Stix's theory.

One very important recent result was obtained during the study of the ICRF-induced pinch [40] of resonating ^{3}He minority ions in D and ^{4}He-plasmas. In this study, toroidally asymmetric ICRF waves were used to modify the orbits and thereby the radial profile of the fast ^{3}He ions. The line-integral measurements of gamma-ray emission along the lines of sight shown in Figure 1 were tomographically reconstructed in order to give the local gamma-ray emissivity in a poloidal cross-section shown in Figure 10. In these reconstructions, the full geometry of the collimators and detectors has been taken into account, but small effects of attenuation and scattering of the gamma rays have been neglected. A constrained optimisation method is used for the tomography. This method is widely used for tomographic reconstructions and has been applied earlier successfully to soft x-ray and bolometer measurements at JET. It is seen in Figure 11 that the emissivity profile in the discharge with -90^{o} phasing is spread out along, and is very narrow across, the ^{3}He cyclotron resonance layer, while in the discharge with $+90^{o}$ phasing the emissivity is much stronger and the profile is spread out on the low field side of the resonance layer. This can be explained by the evolution of the guiding centre orbits of resonant ions during ICRH [40]. Analysis of the gamma-ray energy spectra measured in these discharges indicates that the gamma radiation is produced mainly by the nuclear reaction $^{12}C(^{3}He,p\gamma)^{14}N$. With $+90^{o}$ phasing, the effective temperature of the ICRF-accelerated ^{3}He-ions is $<T_{eff}>=650 \pm 150$ keV. For discharge with opposite (-90^{O}) phasing, $<T_{eff}>$ is roughly the same, but the total gamma-radiation intensity is halved, consistent with the gamma-emission profile measurements.

The experiments were performed in ^{4}He-plasma with deuterium as a minority. This is the case of favourable background conditions, which we use for the precise γ-ray measurements [22]. Spatial profiles of the γ-ray emission in the energy range $E_{\gamma}>1$ MeV have been measured using the Gamma

Cameras with *CsI(Tl)* photo-diode array and data acquisition system which accommodates the γ-ray measurement in four independently adjustable energy windows as it has been described above. The energy windows, containing the 3.09 MeV and 4.44 MeV peaks with their single and double escape satellites were set up to measure spatial profiles of the γ-ray emission from *D* and ^4He-ions. A typical example of the tomographic reconstruction of the measured line-integrated profiles recorded during 1s in a steady state phase of the plasma discharge is shown in Figure 12. It is seen clearly that the γ-ray emission profile produced by fast *D*-ions (right-hand figure) differs from the profile from ^4He-ions (left-hand figure). This effect can be explained by the difference in pitch-angle distribution between ^4He beam-ions injected into the plasma quasi-tangentially and isotropic *D*-minority ions. Furthermore, the *D*-minority ions, unlike the ^4He-ions, produce γ-rays in the broad band of energies, and so the *D*-ions with different orbit topologies contribute to the γ-ray emission profile. The ability of the Gamma Cameras to separate γ-rays from different energy bands allows the study of the fast ion behaviour in some important plasma scenarios.

8. GAMMA RAY DIAGNOSTICS OF ICF PLASMAS

The discussion in the preceding sections has focused on magnetically confined fusion (MCF) plasmas. Gamma ray diagnostics have likewise been brought to bear on the study of inertially confined fusion (ICF) plasmas. This effort has focused principally on the 16.7 MeV gamma ray from the reaction $D(T,\geq)^5He$. As discussed in section vi above, the observation of this gamma ray from quasi-steady state MCF plasmas is fraught with difficulty by virtue of the overwhelming flux of 14 MeV neutrons (the neutron to gamma ray ratio at the relatively low energies is about 10^5:1). This difficulty can, in principle, be circumvented in the case of ICF plasmas by virtue of the signficantly greater speed of the fusion gamma rays (0.30 m/ns) compared to that of the 14MeV neutrons (0.052 m/ns). In practice this has been achieved using a gas Cherenkov detector boasting a time resolution of a few hundred picoseconds and an energy discriminator of 12 MeV [41]. This detector has been used observe the *DT* fusion gamma rays from the Omega facility and promises to play an important diagnostic role in the U.S. National Ignition Facility (NIF) [42]

9. FUTURE POSSIBLE APPLICATIONS OF FUSION GAMMA RAY SPECTROMETRY

In a long-term perspective, fusion alpha-particle measurements with 2-D cameras could be used in the next step burning plasma devices such as ITER. However the γ-ray detectors should be protected against severe neutron emission with special neutron filters [31]. Since the main impurity in ITER plasmas will probably be beryllium, the slowed deuterons will give rise to gammas (2.88 MeV and 3.37 MeV) from the $^9Be(d,n\gamma)^{10}B$ and $^9Be(d,p\gamma)^{10}Be$ reactions, whereas the fusion alphas with energies around the 2-MeV resonance in the $^9Be(^4He,n\gamma)^{12}C$ reaction produce 4.44-MeV gammas. Using γ-ray spectrometers in every channel of the ITER cameras, the α-particle slowing down profile can be measured with the technique successfully tested in JET Trace Tritium Experiments [23]. Simultaneous measurements of the NBI power deposition and α-particle slowing down profiles

are very important for the optimisation of different plasma scenarios and understanding of the fast-ion confinement effects for further progress on the way to *DT*-ignition.

Well beyond the next step burning *DT* plasmas, the aneutronic plasmas such as *p-Li* and *p-B* will certainly rely on the associated capture gamma rays as the principal diagnostic of the primary energy producing nuclear reactions as all of the baryonic fusion products will be charged and hence, one would hope, magnetically confined.

ACKNOWLEDGEMENTS

This work was funded jointly by the U.S. Department of Energy grant DE-FG03-95ER54303, by the United Kingdom Engineering and Physical Sciences Research Council and by the European Communities under the contract of Association between EURATOM and UKAEA. The views and opinions expressed herein do not necessarily reflect those of the European Commission. This work has been carried out within the framework of the European Fusion Development Agreement.

REFERENCES

[1]. F.C. Young J. Golden and K. Kapetanekops, Rev. Sci. Instrum. **48** (1977) 432.

[2]. S.S. Medley and H. Hendel, Bulletin of the American Physical Society, **26** (1982) 982 and PPPL Report #1950 (1980).

[3]. F.E. Cecil and D.E. Newman, Nucl. Instrum. Methods. **221** (1984) 449.

[4]. D.E. Newman and F.E. Cecil, Nucl. Instrum. Methods **227** (1984) 339.

[5]. F.E. Cecil and F.J. Wilkonson III, Physical Review Letters **53** (1984) 767.

[6]. G.L. Morgan, P.W. Liskowski, S.A. Wender, R.E. Brown, N. Jarmie, J.F. Wilkerson and D.M. Drake, Physical Review. **C33** (1986) 1224.

[7]. J.E. Kammerad, J. Hall, K.E. Sale, C.A. Barnes, S.E. Kellog and T.R. Wang, Physical Review **C47** (1993) 29.

[8]. F.E. Cecil, D.M. Cole, R. Philbin, N. Jarmie and R. Brown, Physical Review **C32** (1985) 690.

[9]. F.J. Wilkinson III and F.E. Cecil, Physical Review **C31** (1985) 2036.

[10]. C.A. Barnes, K.H. Chang, T.R. Donoghue and C. Rolfs, Physics Letters **B197** (1987) 315.

[11]. G.J. Sadler, O.N. Jarvis, P. v. Bell, N. Hawkes and B. Syme, 14th European Conference on Controlled Fusion and Plasma Physics (Madrid). (European Conference Abstracts) vol III (1987) 1232.

[12]. D.A. Boyd, D.J. Campbell, J.G. Cordey, W.G.F. Core, J.P. Christiansen, G.A. Cottrell, L.G. Eriksson, T. Hellsten, J.J. Jacquinot, O.N. Jarvis, P.R. Thomas, P. v. Belle, and J.A. Wesson, Nuclear Fusion **29** (1989) 593.

[13]. F.E. Cecil and S.S. Medley, Nucl. Instrum. Methods **271** (1989) 628.

[14]. T. Nishitani, K. Tobita, Y. Kusama, and Y. Shibata, Rev. Sci. Instrum. **72** (2001) 887

[15]. F.E. Cecil, H. Liu, D. Ferg, J.A. McNeil and P.D. Kunz, Nucl. Physics **A539** (1992) 75.

[16]. F.E. Cecil, H. Liu, J.C. Scorby and S.S. Medley, Rev. Sci. Instrum. **61** (1990) 3223.
[17]. F.E. Cecil, S.J. Zweben and S.S. Medley, Nucl. Instrum. Methods **245** (1986) 547.
[18]. V.G. Kiptily, Fusion Technology **18** (1990) 583.
[19]. O.N. Jarvis, J.M. Adams, P.J.A. Howarth, F.B. Marcus, E. Righi, G.J. Sadler, D.F.H. Start, P. v. Belle, C.D. Warrick and N. Watkins, Nucl. Fusion**36** (1996) 1513.
[20]. V.G. Kiptily, F. E. Cecil, O.N. Jarvis, M.J. Mantsinen, S.E. Sharapov, L. Bertalot, S. Conroy, L.C. Ingesson, T. Johnson, K.D. Lawson, S. Popovichev, Nucl. Fusion **42** (2002) 999.
[21]. V.G. Kiptily, S. Popovichev, S.E. Sharapov, L. Bertalot, F.E. Cecil, S. Conroy and M.J. Mantisen, Rev. Sci. Instrum. **74** (2003) 1753.
[22]. V. G. Kiptily, J. M. Adams, L. Bertalot, A. Murari, S.E. Sharapov, V. Yavorskij, B. Alper, R. Barnsley, P. de Vries, C. Gowers, L.-G. Eriksson, P. Lomas, M. J. Mantsinen, A. Meigs,1 J.-M. Noterdaeme, F.P. Orsitto, Nucl. Fusion **45** (2005) L21-L25.
[23]. V.G. Kiptily, Yu.F. Baranov, R. Barnsley, L.Bertalot, N.C. Hawkes, A. Murari, S. Popovichev, S.E. Sharapov, D. Stork, V. Yavorskij. Phys. Rev. Lett. **93** (2004) 115001
[24]. F.E. Cecil, H. Liu, J. C. Scorby, Rev. Sci. Instrum. **61** (1990) 3223.
[25]. S.S. Medley, F.E. Cecil, D. Cole, M.A. Conway, and F.J. Wilkinson, III, Rev. Sci. Instrum. **55** (1985) 975.
[26]. S.S. Medley, S.D. Scott, A.L. Roquemore, and F.E. Cecil, Rev. Sci. Instrum. **61** (1990) 3226.
[27] J. M. Adams, O. N. Jarvis, G. J. Sadler, D. B. Syme, N. Watkins, Nucl. Instrum. Methods Phys. Res. **A239** (1993) 277.
[28] F.E. Cecil, P. van Belle, O.N. Jarvis and G.J. Sadler, Preprint JET-IR(94)04
[29] V.G. Kiptily, A.V. Matjukov, A.S. Mishin, V.O. Naidenov, I.A. Polunovskij, L.A. Rassadin and I.N. Chugunov, Fusion Technology **22** (1992) 454.
[30] V.G. Kiptily, I.N. Chugunov, V.O. Naidenov, I.A. Polunovskij and A.E. Shevelev, Plasma Devices and Operations **7** (1999) 255.
[31] V.G.Kiptily, A.V. Livke, V.I. Nagorny, Yu.Ya. Nefedov, M.V. Savin, V.I. Semenov, V.A. Chirkin, Soviet Physics - Technical Physics **43** (1998) 471.
[32] T. Kondoh, A. Nagashima, Y. Tsukahara, R.K. Richards, D.P. Hutchinson, S. Moriyama, A. Morioka, K. Tobita, Y. Kusama, V.G. Kiptily, 1998 ICPP & 25th European Conference on Controlled Fusion and Plasma Physics (Praha). ECA Vol. **22C** (1998) 1478.
[33] G. J. Sadler, S. W. Conroy, O. N. Jarvis, et al., Fusion Tech. **18**, (1990) 556.
[34] V.G.Kiptily, T.Kondoh, V.O.Naidenov, I.A.Polunovski, Yu.V.Tuboltsev, I.N.Chugunov, A.E.Shevelev, Gamma Ray Spectrometry in ITER: Conceptual Design // in: Diagnostics for Experimental ThermoNucl. FusionReactors 2, P.E.Stott, G.Gorini, E.Sindoni, eds., Plenum Press, New York & London, 1998.
[34]. V.G.Kiptily, S.M. Taova, A.G. Zvenigorodskii, Database for Works on Gamma-diagnostics of Tokamak Plasma // in: Diagnostics for Experimental ThermoNucl. FusionReactors 2, P.E. Stott, G. Gorini, E. Sindoni, eds., Plenum Press, New York & London, 1998.

[36]. M.J. Mantsinen, O.N. Jarvis, V.G. Kiptily et al., Nucl. Fusion **41** (2001) 1815.
[37]. J. Jacquinot, G.J. Sadler, Fusion Technology **21** (1992) 2254.
[38]. M.J. Mantsinen, M.-L. Mayoral, V.G. Kiptily et al., Phys. Rev. Lett. **88** (2002) 105002.
[39]. V. G. Kiptily et al. 31st EPS Conference on Plasma Phys. London, 28 June - 2 July 2004 ECA Vol.28G, O-1.06 (2004)
[40]. M. J. Mantsinen, L. C. Ingesson, T. Johnson, V. G. Kiptily et al., Phys. Rev. Lett. **89** (2002) 115004.
[41]. R.R. Bergran, S.E. Caldwell, J.R. Falukner Jr., R.A. Lerche, J.M. Mack, K.J. Moy, J.A. Oertel and C.S. Young, Rev. Sci. Instruments **72** (2001) 873.
[42]. S.E. Caldwell et al. Rev. Sci. Instruments **74** (2001) 1837.

Reaction	**Q-value (MeV)**	**S(0) keV-b**	**_ (MeV)**
$D(p,\gamma)^3He$	5.5	.00023 +/- .00001	0.0
$T(p,\gamma)^4He$	19.7	.0013 +/- .0003	0.0
$D(d,\gamma)^4He$	23.8	.000011+/-.000003	0.0
$D(t,\gamma)^5He$	16.63	0.63 +/- 0.15	0.60
$D(^3He,\gamma)^5Li$	16.38	0.26 +/- 0.07	1.5

Table 1 Properties of direct fusion gamma ray reactions

Reaction	Energy of reaction, Q,	MeV E_{min}, MeV *)
	Protons	
$D(p,\gamma)^3He$	5.5	0.05
$T(p,\gamma)^4He$	19.81	0.05
$^9Be(p,p'\gamma)^9Be$	-2.43	3
$^9Be(p,\gamma)^{10}B$	6.59	0.3
$^9Be(p,\alpha\,\gamma)^6Li$	2.125	2.5
$^{12}C(p,p'\gamma)^{12}C$	-4.44, -7.65	5, 8
	Deuterons	
$^9Be(d,p\gamma)^{10}Be$	4.59	0.5
$^9Be(d,n\gamma)^{10}B$	4.36	0.5
$^{12}C(d,p\gamma)^{13}C$	2.72	0.9
	Tritons	
$D(t,\gamma)^5He$	16.63	0.02
$^9Be(t,n\gamma)^{11}B$	9.56	0.5
	^{3}He-ions	
$D(^3He,\gamma)^5Li$	16.38	0.1
$^9Be(^3He,n\gamma)^{11}C$	7.56	0.9
$^9Be(^3He,p\gamma)^{11}B$	10.32	0.9
$^9Be(^3He,d\gamma)^{10}B$	1.09	0.9
$^{12}C(^3He,p\gamma)^{14}N$	4.78	1.3
	Alphas	
$^9Be(^4He,n\gamma)^{12}C$	5.70	1.9

*) - Assessment of the minimal fast particle energy needed for gamma-ray observation at JET

Table 2: Nuclear reactions identified in gamma-ray spectra recorded at JET [20].

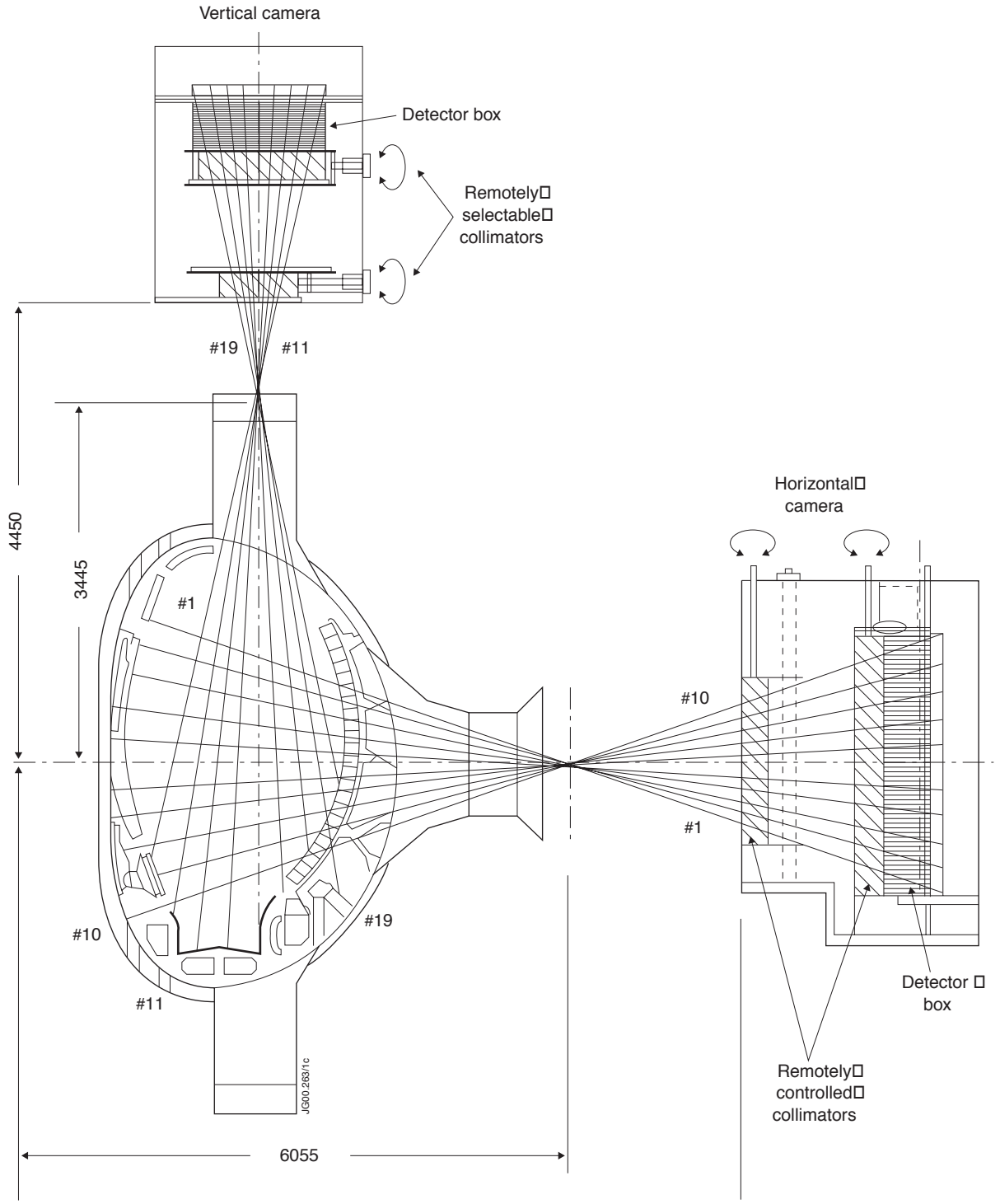

Figure 1 Schematic of the JET neutron emission profile monitor used for the spatial gamma-ray emissivity measurements [27].

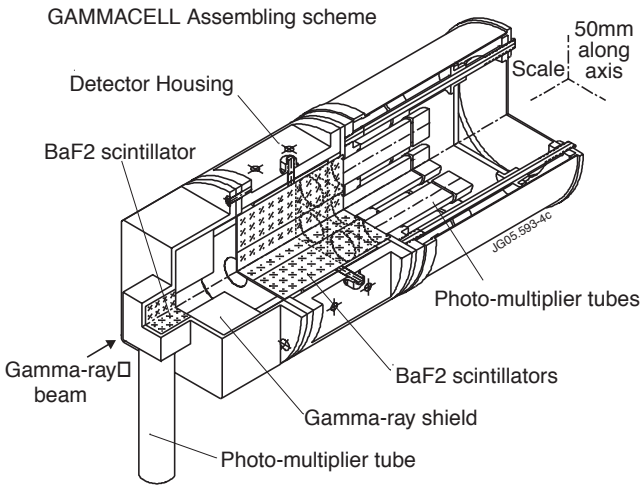

Figure 2: Scheme of the GAMMACELL detector system [30].

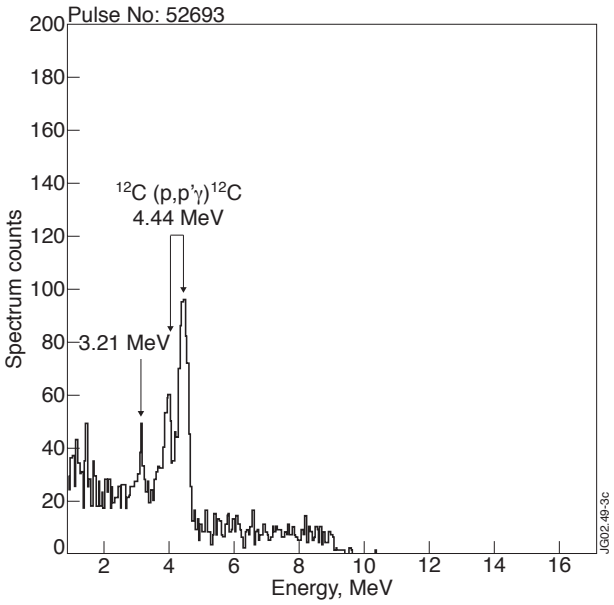

Figure 3: Gamma-ray spectrum measured during discharge with ICRF heating tuned to $\omega=\omega_{cH}$ in deuterium JET plasma [20].

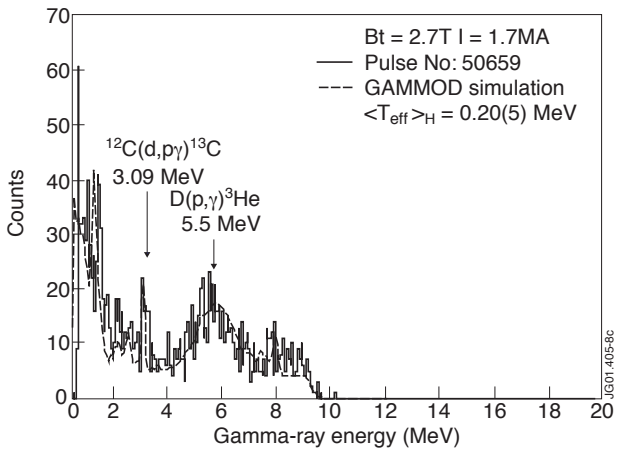

Figure 4: Gamma-ray spectrum measured during JET discharge with ICRF heating tuned to $\omega=\omega_{cH}$ in deuterium JET plasma. The spectrum calculated by means of the program GAMMOD (dashed line) [19].

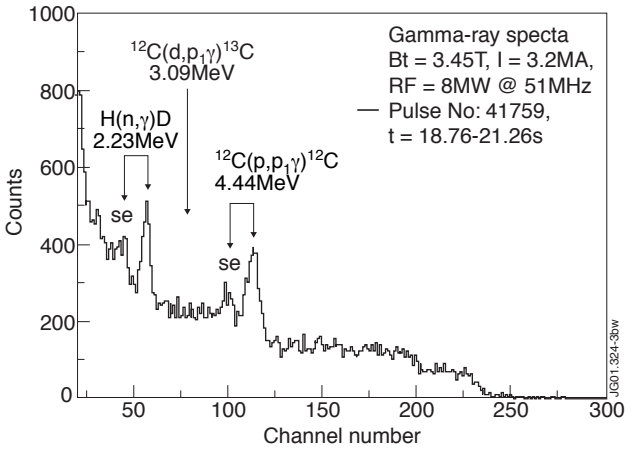

Figure 5: Gamma-ray spectra measured during tritium discharge with H-minority heating; $T_e(0) \cong 9keV$, $n_e(0) \cong 2.5 \times 10^{19}\ m^{-3}$, ICRF frequency $f = 51MHz$, $P_{ICRF} \cong 8MW$, relative deuterium density $\eta_D \cong 5\%$, relative hydrogen density $\eta_H \cong 5\%$. The energy scale of the spectrum is given by $E_\gamma(MeV) = 0.0385+0.0937*N$, where N is channel number [33].

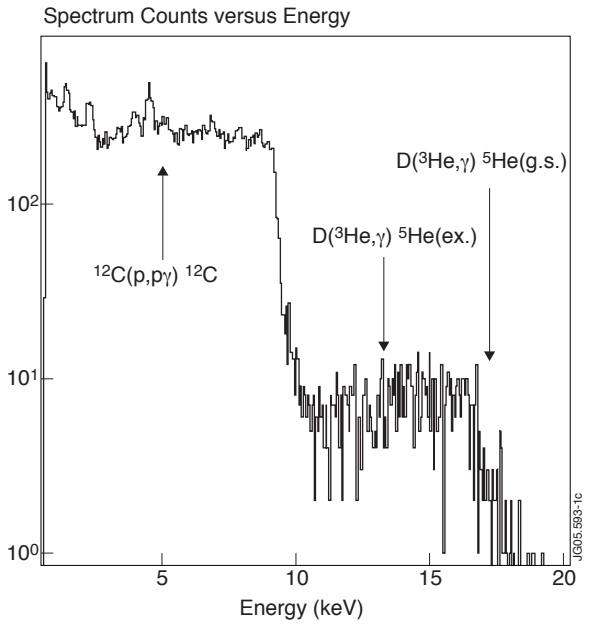

Figure 6.: Gamma-ray energy spectra measured during 4 discharges with ICRF heating tuned to $\omega=\omega_{c3He}$ in deuterium JET plasma with ^{3}He-minority. The ^{5}Li ground and first excited state are not resolved due to the intrinsic widths of the gamma rays.

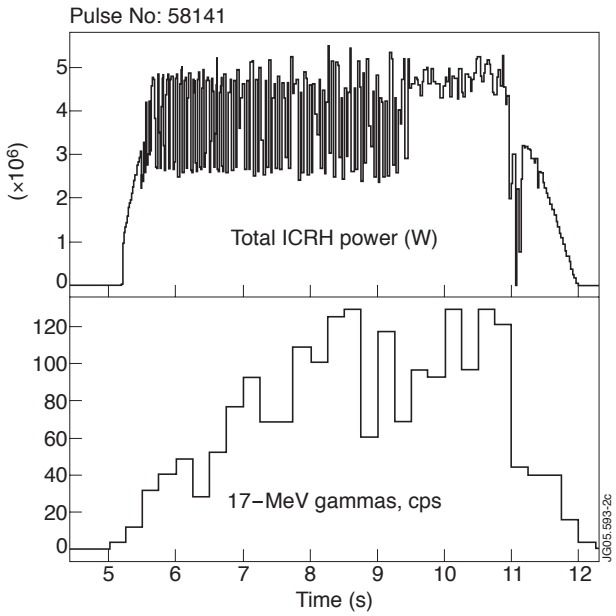

Figure 7: Typical count rate of 17-MeV gamma-rays recorded in JET in the mode conversion experiments with ^{3}He-minority (4%) ICRF heating.

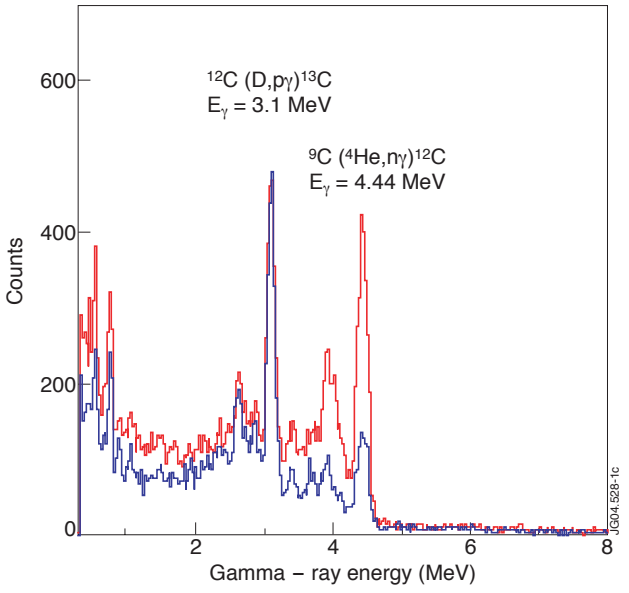

Figure 8: Gamma-ray spectra measured by the NaI(Tl) detector: (solid line) spectrum recorded in discharge with 70keV and 110keV ^{4}He-beam injectors; (dash line) spectrum recorded in a discharge with two 70keV ^{4}He-beam injectors [38].

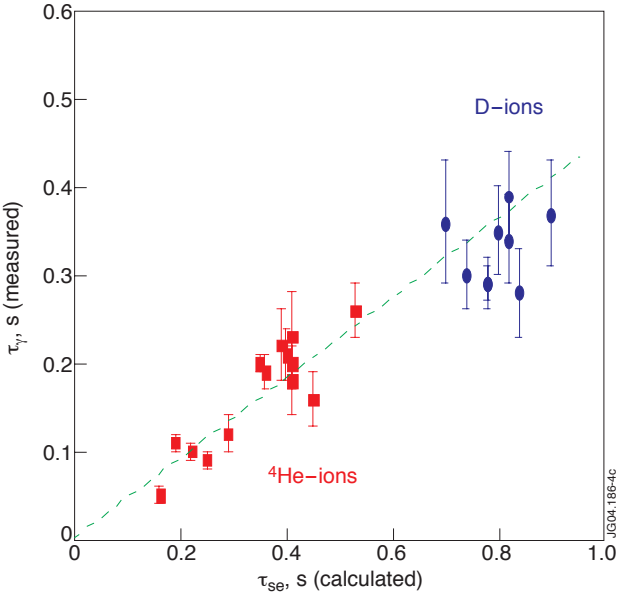

Figure 9: Comparison of decay-times of 4.44MeV γ-rays from the ^{9}Be(^{4}He,nγ)^{12}C reaction and 3.09MeV γ-rays from the reaction ^{12}C(d,pγ)^{13}C .

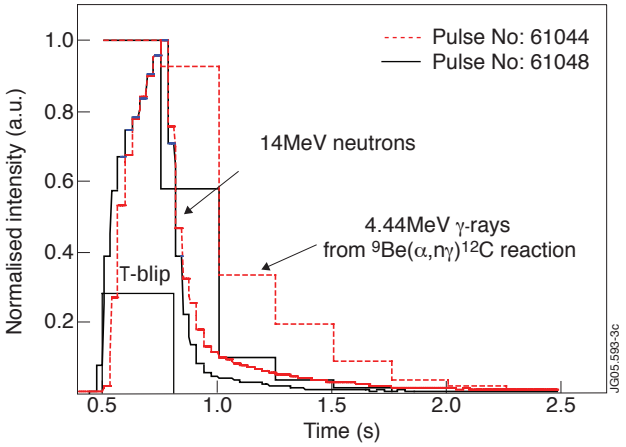

Figure 10: Comparison of time evolutions of 4.44-MeV γ-ray emission and 14-MeV neutrons measured in the 2.0MA/ 2.25T discharges 61044 and 61048 [22]. Pulse No. 61044: $P_{DNBI} \cong 14.5$ MW $P_{TNBI} \cong 1.5$MW. Pulse No. 61048: $P_{DNBI} \cong 2.9$ MW $P_{TNBI} \cong 2.3$MW.

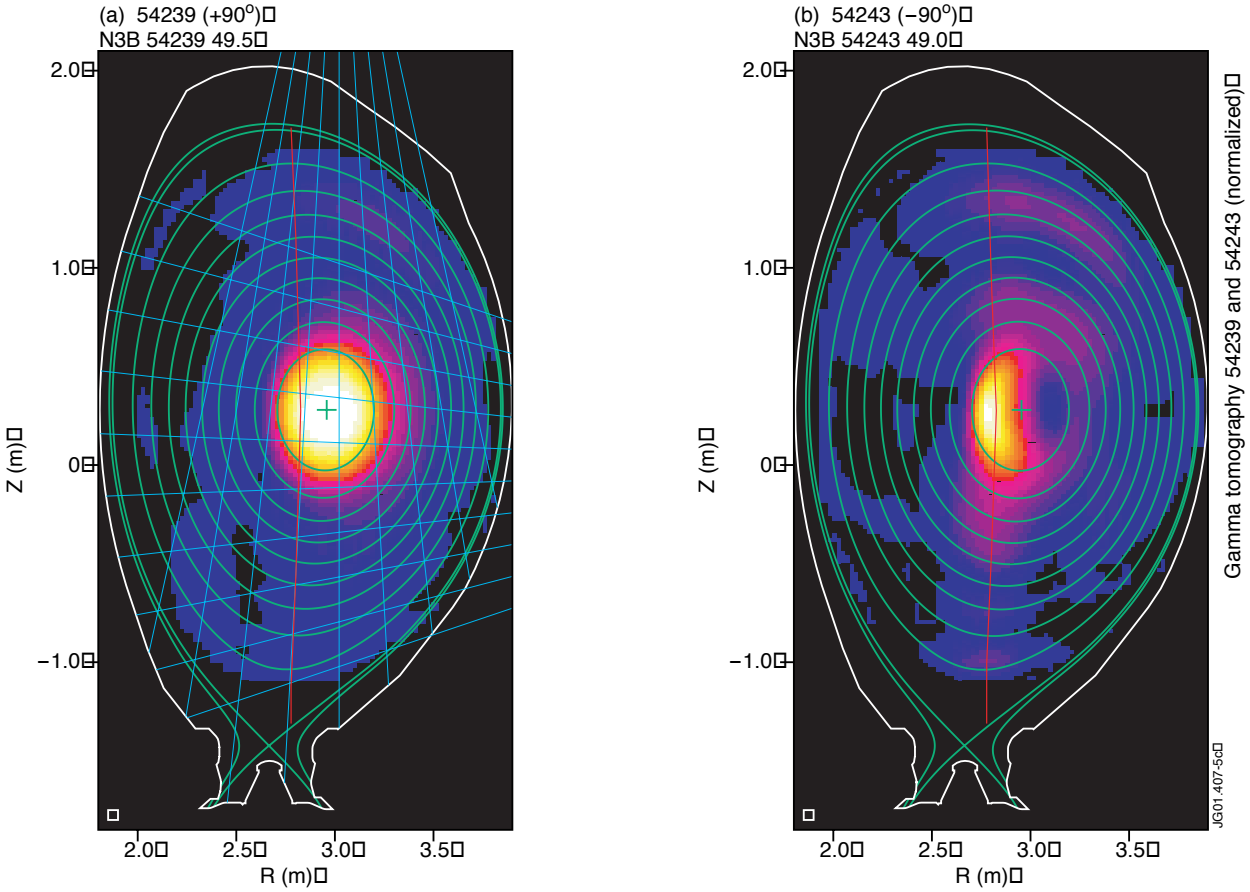

Figure 11: Reconstructed gamma-ray emission profiles (normalised to the peak values) for discharges with ICRF heating of ^{3}He minority (1-2%) ions using -90^{o} and $+90^{o}$ phasing of the JET ICRF antennas, f = 37MHz, $P_{ICRF} \cong$ 7MW [19]. The lines of sight of the profile monitor are indicated by blue lines. A number of flux surfaces are shown in green; the magnetic axis is indicated by a cross. The location of the resonance layer is indicated by a red line. The box in the lower-left corner indicates the grid size used in the tomographic reconstructions.

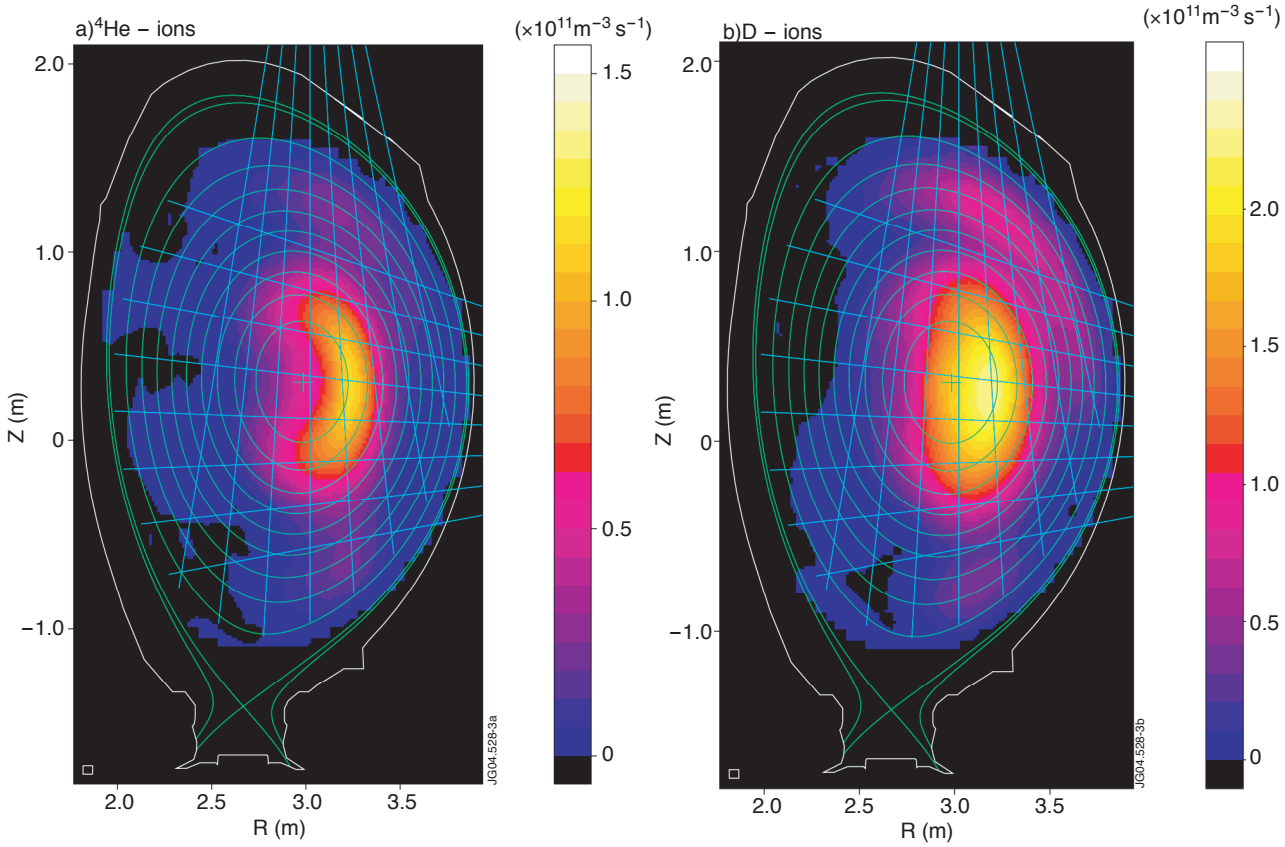

Figure 12: Tomographic reconstructions of 4.44MeV γ-ray emission from the reaction $^{9}Be(^{4}He,n\gamma)^{12}C$ (left) and 3.09MeV γ-ray emission from the reaction $^{12}C(D,p\gamma)^{13}C$ (right) deduced from simultaneously measured profiles [22].